Synchronization of two bubble trains in a viscous fluid: Experiment and numerical simulation

Felipe Augusto Cardoso Pereira,[1] Eduardo Colli,[2] and José Carlos Sartorelli[1]
[1]*Instituto de Física, Universidade de São Paulo, Caixa Postal 66318, 05315-970 São Paulo, Brazil*
[2]*Instituto de Matemática e Estatística, Universidade de São Paulo, Rua do Matão, 1010, 05508-090 São Paulo, Brazil*
(Received 1 November 2012; published 28 February 2013)

We investigate the interactions of two trains of bubbles, ejected by nozzles immersed in a viscous fluid, due only to the solution's circulation. The air fluxes (Q_1,Q_2) are controlled independently, and we constructed parameter spaces of the periodicity of the attractors. We have observed complex behavior and many modes of phase synchronization that depend on these airflows as well as on the height (H) of the solution above the tops of the nozzles. Such synchronizations are shown in details in the parameter space (Q_1,Q_2) and also in the (Q_1,H) space. We also observed that the coupling strength between the two trains of bubbles increases when the solution height increases. The experimental results were reasonably explained by numerical simulations of a model combining a simple bubble growth model for each bubble train and a coupling term between them, which was assumed symmetrical and proportional to the growth velocities.

DOI: 10.1103/PhysRevE.87.022917 PACS number(s): 05.45.Xt, 05.45.Pq, 47.55.db

I. INTRODUCTION

Synchronization may appear in any nonlinear system composed of a group of coupled oscillators or by a self-sustained oscillator that is subject to an external force [1]. It has been observed in biological processes [2], such as ecological systems [3], postural control [4] and the cardiorespiratory system in humans [5], coupled neurons [6,7], and neuron networks [8]. Synchronization of coupled chaotic systems has been seen as a way to improve secure communications, complementing software encryption [9,10].

The frequency-locking synchronization of the bubbling of a single nozzle with a periodic external force (a sinusoidal sound wave) was studied in Refs. [11–13] and synchronized regions were identified. For most of the synchronization regions found, the bubbling frequency was a submultiple of the sound frequency, since the parameter windows are usually wider than in higher-order synchronizations. Some experiments showed synchronizations with four different submultiples, with sound frequencies four to ten times the frequency of the bubbling. Chaos arising for strong enough external forces was also studied. As the gas-liquid reactors usually have multiple orifices or nozzles many studies on synchronization in air bubbling has been done in systems with two or more orifices in the same plenum [14–16]. It was shown that the synchronization depends on the distance between the orifices [15] and two synchronized modes were found, one for the low-airflow regime and another for higher airflow, with nonperiodic behavior (intermittence) in between them [16]. These systems have behavior that is difficult to predict since the bubbling orifices are coupled both by the common air reservoir and by the fluid above. In Ref. [17], Snabre and Magnifotcham studied the effect of adding an independent bubble stream next to a previously ongoing one. They showed that the rising velocity of the ongoing bubble stream is reduced as the airflow of the added nozzle increases, and that the bubble streams attract each other, causing a small deviation of the bubble paths from the vertical.

We present experimental results of phase synchronization of two bubbling streams, generated in two nozzles with independent airflow controls, interacting only via the solution's circulation. In this particular setup, the bubble train generated in each nozzle has a period-1 regime, in the whole air flux range, when each one is bubbling alone. The experiments have the airflows Q_1 and Q_2 of both nozzles and the fluid height H above the nozzle tops as control parameters. The airflow establishes the natural bubbling frequency, and we also show that the fluid height above the nozzles increases the size of the periodic (synchronized) regions in the parameter space (Q_1,Q_2). For each nozzle we used a simple model for bubble formation, developed by us and described in Ref. [18]. In the present case of the interaction of bubbles formed in each nozzle, we insert a symmetric coupling between them that is proportional to the growth velocities of the bubbles. This model reproduces the experimental parameter spaces, with the coupling strength playing the same role as the solution height in the experiment.

II. EXPERIMENTAL APPARATUS

A diagram of the experimental apparatus is shown in Fig. 1. It consists of an acrylic transparent cylindrical container of 10 cm diameter which is partially filled with a glycerol and water solution (75%–25%). The bubbles are generated by injecting air through two symmetrically placed nozzles at the bottom of the solution container. Each nozzle is the tip of a hypodermic syringe, without needle, with a channel of length 10 mm and internal radius 1.1 mm. The bubbles appear at the nozzles 4.5 cm above the bottom of the cylinder and 4.5 cm away from each other. Each nozzle is connected to an independent air injection system, with its airflow rate Q controlled by a proportional solenoid valve driven by a proportional-integral-derivative (PID) controller [11,12,19] and measured with a mass flow meter in ml/min. These geometrical parameters of the individual nozzles are similar to the ones used in Ref. [13], where the bubbling regime is such that the time between bubbles is constant.

In each nozzle, the time delay T_i between successive bubbles was obtained by detecting in a resistor the beginning of the 5 V voltage pulses induced by the scattering of a laser beam (placed a little above the nozzle), focused in a photodiode which is in series with the resistor. The bubbling frequency is

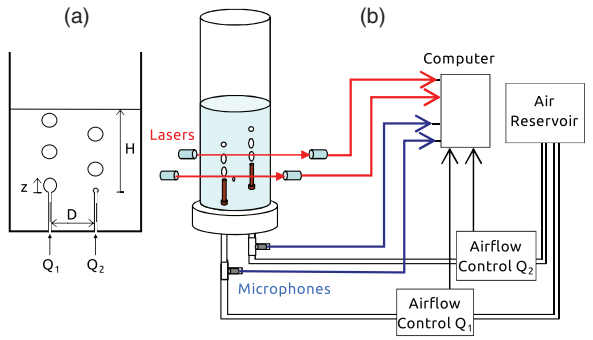

FIG. 1. (Color online) Schematic drawing of the experimental apparatus. (a) Enlargement of the cylindrical container showing the relevant parameters: The distance between the nozzles D, the solution height H above the nozzle tops, the airflows Q_1 and Q_2 to both nozzles, and the height z of the bubble on the nozzle. (b) Overview of the experimental setup, showing the air reservoir and the two air injection systems, with the independent airflow controllers. The microphones are used to detect the pressure wave and the laser beams are used to detect the time interval between bubbles, T_i.

defined as $f^{(k)} = \langle T_i^{(k)} \rangle^{-1}$, where $k = 1,2$. The pressure waves created by the bubbling inside each hose were detected with microphones [18], whose signals are proportional to $-\dot{p}$. All data were collected by a data acquisition system composed of eight analog-to-digital converters (ADCs) of 16 bits at 250 000 samples/s measuring the signals simultaneously, allowing comparison of the signals from both nozzles.

Bifurcation diagrams are constructed by plotting the T_i from each nozzle in different colors (gray scale) against the air flow Q_1, allowing it to vary at the rate of 4.0 ml min^{-2}, by using the linear ramp mode of the PID set point. These diagrams are obtained for different values of the airflow of the second nozzle Q_2, as well as the solution height H above the nozzle tops. We also constructed parameter spaces showing the periodicities and synchronizations with colors (gray scale) with different textures. The bubble formation regimes from each nozzle were analyzed by determining the periodicity from the time series $T_i^{(k)}$ and the synchronization of the two regimes from the microphone signals. Two kinds of parameter space were drawn: (Q_1, Q_2), for fixed values of H, and (Q_1, H), for fixed values of Q_2.

III. RESULTS AND DISCUSSION

A. Experimental results

1. Bifurcation diagrams

Letting the air flow (Q_1 or Q_2) vary in the [40, 180] ml/min interval, the bubbling in each isolated nozzle occurs at fixed time intervals or at the same bubbling frequencies, which characterize the period-1 behavior. However, when both nozzles are bubbling together complex behaviors appear, with regions of higher periodicity and nonperiodicity, depending on both airflows (Q_1 and Q_2) as well as on the solution height (H) above the nozzles. In Fig. 2 is shown a bubbling example for $H = 80$ mm. In both nozzles we have periodic behaviors at different airflows $Q_1 = 160$ ml/min (left nozzle) and $Q_2 = 60$ ml/min (right nozzle). The bubbling frequencies

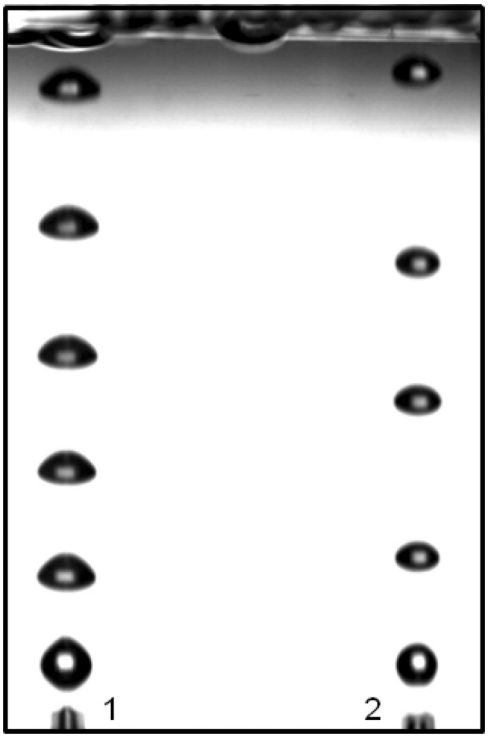

FIG. 2. A snapshot of a bubbling example of frequency locking 2:3 (see the movie in the Supplemental Material [20]), for $H = 80$ mm, $Q_1 = 160$ ml/min, and $Q_2 = 60$ ml/min. In nozzle 1 there are three different values of the time intervals between successive bubbles while in nozzle 2 only two values are observed.

are $f_1 \approx 27.5$ bubbles/s and $f_2 \approx 18.3$ bubbles/s, whose ratio $f^{(2)}/f^{(1)} \approx 0.66$ indicates a 2:3 frequency locking of bubbles of different sizes.

In Fig. 3, we show bifurcation diagrams $T_i^{(1)}$ vs Q_1 and $T_i^{(2)}$ vs Q_1 obtained by slowly increasing the airflow Q_1 of the first nozzle at a rate of 4 ml min^{-2} while keeping the second nozzle airflow constant at $Q_2 = 105$ ml/min. The diagrams presented in Fig. 3(a) for $H = 120$ mm have large windows of period 1 in the range [85, 118] ml/min which is a 1:1 frequency locking, since only one value of the time intervals between successive bubbles was observed in both nozzles. Other periodic windows can be seen, such as for Q_1 in the range [40, 48] ml/min. In this case, the bubbling in nozzle 1, shown in magenta (light gray), presents two distinct values of $T_i^{(1)}$, so it is a period-2 behavior, while the bubbling in nozzle 2, shown in black, presents three distinct values of $T_i^{(2)}$, so it is a period-3 regime. Therefore, for these parameters, we have a 2:3 frequency locking. The same conclusion can be reached by calculating the ratio of bubbling frequencies $f^{(1)}/f^{(2)} = \langle T^{(2)} \rangle / \langle T^{(1)} \rangle \cong 0.67$ [see Eq. (4)]. For Q_1 around 170 ml/min, the ratio of bubbling frequencies $f^{(1)}/f^{(2)} \cong 1.2$ indicates a 6:5 frequency locking.

In the case of Fig. 3(b) for $H = 30$ mm, only the frequency-locking window 1:1 is clearly seen in the range [100, 110] ml/min with the same time intervals between successive bubbles in both nozzles. Other windows are more difficult to detect, since the width of the time interval $\delta T = \max(T) - \min(T)$ is too small, approximately 1.5 ms, while the periodicities P were determined by counting the number

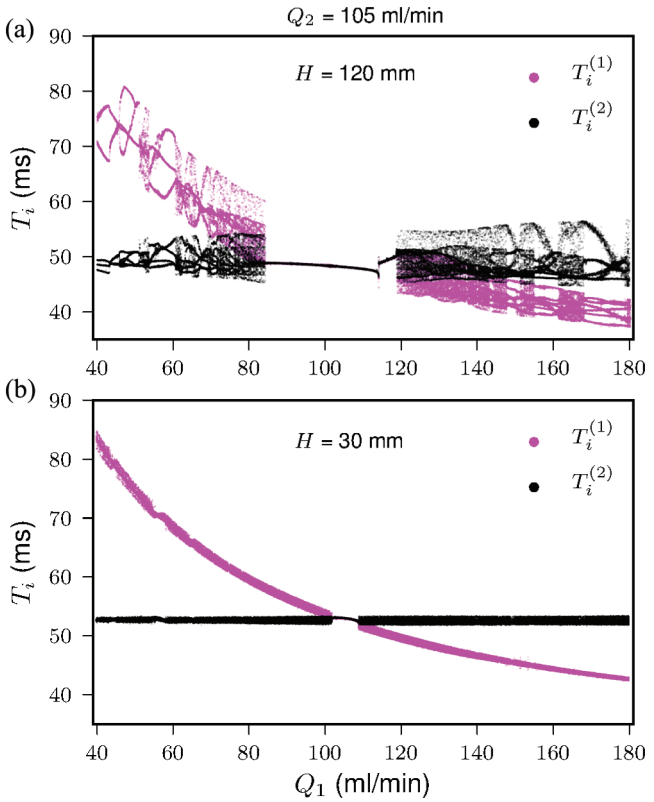

FIG. 3. (Color online) Experimental bifurcation diagrams obtained by slowly changing the airflow, at the rate of 4 ml/min^2, of the first nozzle Q_1 and for $Q_2 = 105$ ml/min, in (a) for the solution height above the nozzles $H = 120$ mm, and in (b) for $H = 30$ mm. In both cases, the data from the first nozzle are in magenta (light gray) and from the second one in black.

of distinct values T_i using the threshold $\sigma_T \approx 0.15$ ms, which is very near the fluctuations due to noise. However, we were still able to find, in the range $Q_1 = [55,58]$ ml/min, the ratio $f^{(1)}/f^{(2)} \cong 1.34$, showing a 4:3 frequency locking.

2. *Parameter spaces*

These results show that there are many periodic behaviors that depend on the three control parameters Q_1, Q_2, and H. For some values of H we constructed parameter spaces and looked for the periodicities by counting the number of different values of the time series $T_i^{(k)}$ in each nozzle, taking into account the precision threshold $\sigma_T \approx 0.15$ ms. The data were obtained in a set of 41 × 41 different pairs of (Q_1, Q_2), with both airflows in the interval [60, 180] ml/min, with steps of 3 ml/min. For every pair we checked the bubbling behavior by attractor reconstruction by observing the first-return maps $T_{i+1}^{(k)}$ vs $T_i^{(k)}$, for $k = 1,2$. Figure 4 shows the parameter space (Q_1, Q_2) for $H = 90$ mm, with colors (gray scale with different textures) used to indicate the period of each bubble train. The parameter spaces from both nozzles have a periodic window of period 1 around the diagonal $Q_1 = Q_2$, with higher periods appearing in stripes on the upper left and lower right of the diagonal, mainly periods 2, 3, and 4. It can be noted that one space is the mirrored version of the other (in regard to the diagonal) and periodic windows appear together in both spaces, i.e.,

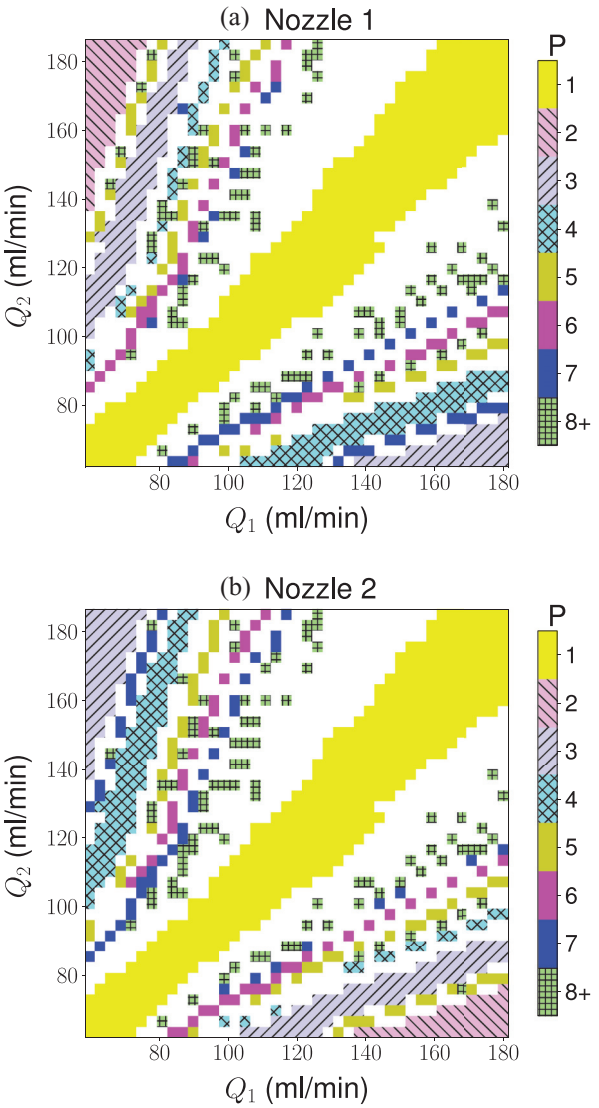

FIG. 4. (Color online) Experimental parameter spaces of the attractor periodicity for the solution height $H = 90$ mm, for (a) nozzle 1 and (b) nozzle 2. The colored regions (gray scale with different textures) show the periodicity P detected, where 8+ represents parameters where the period was 8 or higher. The parameter regions with no periodicity detected are in white.

the parameter region in which there is a periodic window in Fig. 4(a) has a corresponding periodic window in Fig. 4(b).

In the set of 41 × 41 pairs of (Q_1, Q_2) we also used microphones to simultaneously measure the pressure wave in each nozzle, obtaining data more appropriate for detecting synchronization. For this purpose, we first defined a phase function for each nozzle k, $k = 1,2$: after obtaining, by the use of a Poincaré map, the instants t_{N_i} of the maximum of the microphone signal, where N_i is the enumeration of these maxima in the series of nozzle k, we defined $\theta_k(t_{N_i}) = 2\pi N_i$ and, for t between t_{N_i} and $t_{N_{i+1}}$,

$$\theta_k(t) = 2\pi N_i + 2\pi \frac{t - t_{N_i}}{t_{N_{i+1}} - t_{N_i}}. \quad (1)$$

This is similar to what was done with spikes of the cardiac signal in Ref. [5] (see Fig. 5 for an illustration).

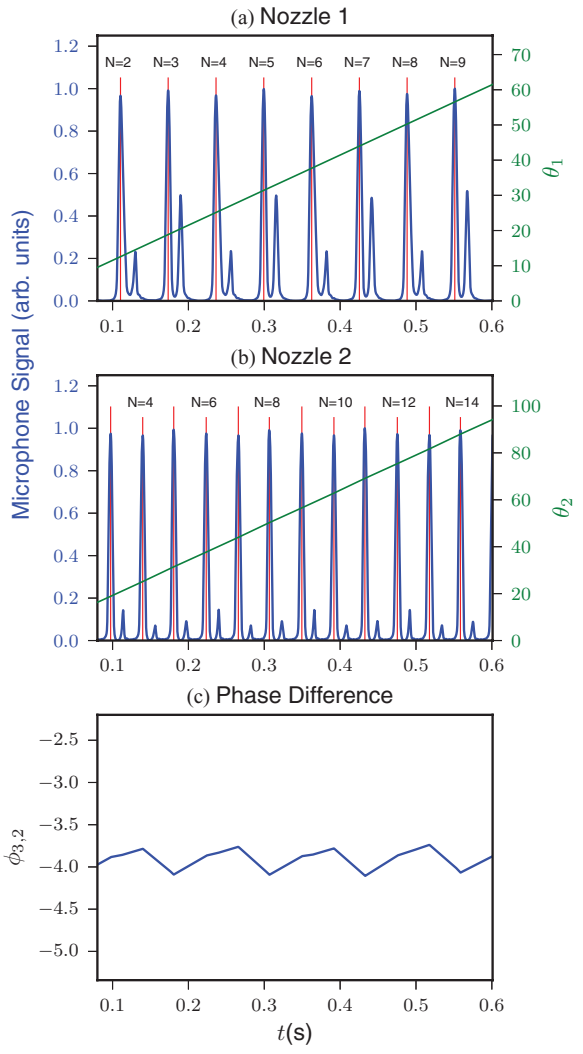

FIG. 5. (Color online) For $Q_1 = 62.9$ ml/min (a) and $Q_2 = 178.7$ ml/min (b), the blue (black) lines are samples of the normalized signals of the microphones, the vertical lines in red (light gray and thin) are the positions of the maxima used to define a phase for each signal, and the green (the oblique straight gray) line (right scale) the phases θ_1 and θ_2 calculated using Eq. (1). (c) The generalized phase difference $\phi_{3,2} = 3\theta_1 - 2\theta_2$ showing that there is a 3:2 synchronization.

Then we used the generalized phase difference [1]

$$\phi_{n,m}(t) = n\theta_1(t) - m\theta_2(t), \tag{2}$$

and we calculated $\phi_{n,m}$ for all combinations of (n,m) with $n,m \leqslant 10$. We looked for the smallest (n,m) such that the absolute value of the phase difference was bounded, i.e.,

$$\phi_{n,m} \leqslant K. \tag{3}$$

The choice of the smallest (n,m) is because when the pair (n,m) satisfies this condition in a system, the pair $(2n,2m)$ will also satisfy it. When $\phi_{n,m}$ is bounded, the system is in an n:m phase-locking synchronization. We have chosen the value for the constant K such that, in a synchronous case, the phase difference $|\phi_{n,m}|$ was smaller than one period of the slower bubbling: $K = 2\pi \max(n,m)$.

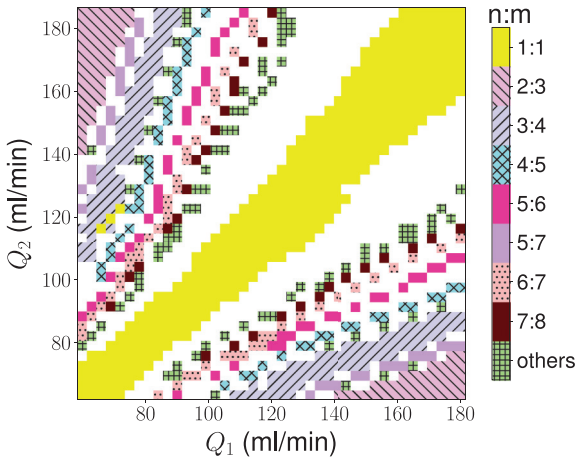

FIG. 6. (Color online) Experimental parameter space (Q_1,Q_2) of the synchronized regions n:m for $H = 90$ mm. This parameter space was built by applying the condition of synchronization given by Eq. (3) to the calculated phase difference Eq. (2). The modes n:m and m:n were painted with the same color (gray scale with the same texture), so the painted regions actually show $\min(n,m) : \max(n,m)$. As the system is symmetric, it is possible to find the right order by looking at the relation between the airflows Q_1 and Q_2. The white regions are the ones with no synchronization found.

It is important to point out that when a system of two oscillators is in an n:m phase synchronization, the mean periods of the oscillators satisfy the relation

$$m\langle T^{(1)}\rangle = n\langle T^{(2)}\rangle, \tag{4}$$

i.e., their frequencies are also locked.

By calculating the generalized phase difference from the microphone time series we made the parameter space for the synchronization that is presented in Fig. 6. To make the space parameters simpler the synchronization space was built by painting the same colors (gray scale with the same texture) for n:m and m:n; otherwise we would have to use twice as many colors to portray the same number of synchronizations. It is important to notice that the decision to give n:m and m:n the same color (gray scale) does not imply a loss of information in the parameter space, as we can recover the order (n:m or m:n) by looking at the airflows Q_1 and Q_2.

The regions of the parameter space in Fig. 6 that have synchronization n:m appear in the parameter spaces of Fig. 4 with periodicity $P_2 = n$ for the bubbling in nozzle 2 and $P_1 = m$ in nozzle 1. For example, the synchronization space shows a 1:1 phase synchronization around the diagonal $Q_1 = Q_2$, where the period-1 window appears on the periodicity space, and the high-order synchronization windows appear symmetrically with respect to the diagonal with the nozzles presenting periods n and m (or m and n). So the parameter spaces in Figs. 4 and 6 confirm that when the system synchronizes in an n:m regime, the periodicity P_k of the bubbling regimes is n for one nozzle and m for the other.

The effect of the solution height H on the bubbling dynamics can be better visualized in the parameter space (Q_1,H) of phase synchronization. In Fig. 7, we show an example of the (Q_1,H) space, constructed keeping $Q_2 = 147$ ml/min. This parameter space was constructed by acquiring the data

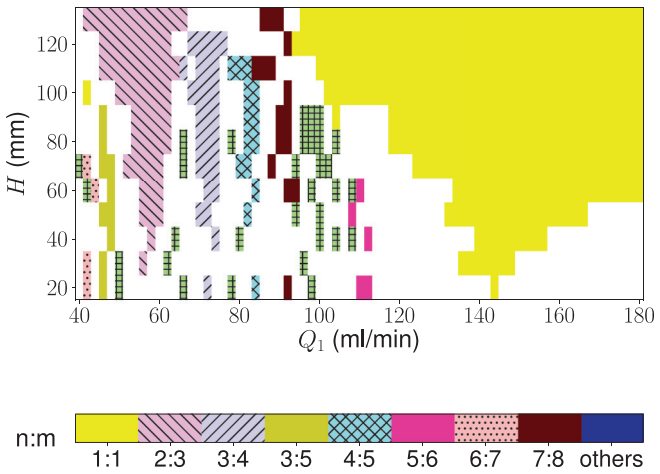

FIG. 7. (Color online) Experimental parameter space (Q_1,H) showing the synchronized regions for $Q_2 = 147$ ml/min. The painted regions show the synchronization detected and the white regions are the ones with no synchronization found.

for combinations of (Q_1,H), keeping the same Q_2 for all measurements, the airflow Q_1 going from 40 to 180 ml/min in steps of 2 ml/min between two consecutive Q_1, and the solution height going from 20 to 130 mm in steps of 10 mm. This made 852 different combinations of (Q_1,H). The 1:1 and 2:3 synchronization modes can be easily recognized in the parameter space (Q_1,H) in Fig. 7. The width of both modes increases as the solution height increases; the 1:1 synchronization window width ranges from 18 ml/min at $H = 40$ mm to 80 ml/min at $H = 130$ mm. The structure of the synchronized regions resembles Arnold tongues, and the parameter space (Q_1,H) in Fig. 7 is similar to the parameter space (Ω,ϵ) of the circle map (see Ref. [13] for Arnold tongues in a bubbling system), where Ω is the ratio of the two oscillator frequencies and ϵ is the strength of the coupling between them. Therefore, we conclude that the interaction between the two bubble trains is stronger when we increase the solution height.

B. Simulation results

To describe the experimental data, we used a model of single-bubble formation developed in Ref. [18]:

$$\begin{aligned} \dot{p} &= \frac{1}{V_0}[RTQ - p\dot{V}(z)] \\ \ddot{z} &= \frac{1}{A(z)}\{[p - p_e(z)] - B(z)\dot{z} - C(z)\dot{z}^2\}, \end{aligned} \tag{5}$$

where p is the pressure inside the reservoir just behind the nozzle, z is the height of the top of the air/solution interface, with $z = 0$ being the top of the nozzle, $p_e(z)$ is the equilibrium pressure, which is the sum of the hydrostatic pressure and the surface tension in the air/solution interface, R,T, and V_0 are constants and $V(z),A(z),B(z),C(z)$ are functions related to the regime of the flow and the geometry of the system; see the Appendix of Ref. [18]. The instants of bubble detachment are given by an equilibrium formula that relates the forces in the bubble: when the upward force (buoyancy) is equal to the downward forces (surface tension and viscous drag).We used the experimental values of the geometrical parameters

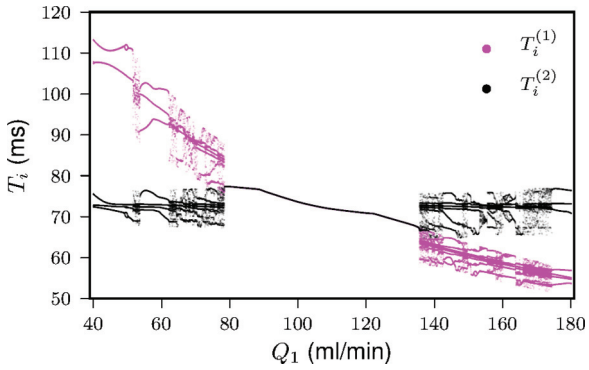

FIG. 8. (Color online) Simulated bifurcation diagrams T_i vs Q_1. The data related to nozzle 1 are shown in magenta (light gray) and for nozzle 2 in black. The airflow of the second nozzle was 105 ml/min, and the coupling constant $\alpha = 26$ kg/m^2 s. The system behavior should be compared with the experimental diagram in Fig. 3(a).

so that an isolated nozzle presents period-1 behavior as in the experiment. As the fluid circulation dynamics has a low Reynolds number, to emulate the interaction between the bubble trains, we added a simple coupling proportional to the velocities of bubble formation in the equilibrium pressure p_e terms:

$$\begin{aligned} \left(p_e^{(1)}\right)_{\text{new}} &= \left(p_e^{(1)}\right)_{\text{old}} + \alpha\dot{z}_2, \\ \left(p_e^{(2)}\right)_{\text{new}} &= \left(p_e^{(2)}\right)_{\text{old}} + \alpha\dot{z}_1, \end{aligned} \tag{6}$$

where α is the strength of the coupling. The bubbles drag the nearby liquid when they go upward, and the liquid goes downward far from them. This velocity profile suggests that the growth of each bubble is inhibited by the bubble of the other nozzle, so the coupling parameters are positive in Eq. (6).

As the coupling was not directly deduced from the properties of the circulating flow, we need to calibrate the value of α. For that, we calculated the distribution $\delta T^{(k)} = \max(T^{(k)}) - \min(T^{(k)})$ as a function of α, Q_1, and Q_2 from numerical integration of the model, and then we compared simulation and experimental data in the nonperiodic regions at the borders of the diagrams ($Q_1 = 40$ and 180 ml/min) for $Q_2 = 100$ ml/min. This calibration gave $\alpha = 22$ kg/m^2 s for $H = 100$ mm.

The bifurcation diagrams for the two nozzles with $\alpha = 26$ kg/m^2 s are shown in Fig. 8. This value was obtained by using the calibration of the constant α for $H = 100$ mm and $\alpha = 0$ for $H = 0$ and doing a linear extrapolation for $H = 120$ mm. The simulated diagram is similar to the experimental one shown in Fig. 3(a). It also shows the 1:1 synchronization window near $Q_1 = Q_2$ and the 2:3 window near $Q_1 = 45$ ml/min.

To detect the synchronization in the simulated system, we made Poincaré maps using the time of detachment. This moment is the most convenient one, as the numerical integration must be halted to reset the initial conditions of the nozzle that the bubble just left.

We have created the synchronization parameter space (Q_1,Q_2) for a constant coupling strength $\alpha = 20$ kg/m^2 s, shown in Fig. 9(a). This value of the coupling α was obtained from the calibration between the numerical simulation and the experimental parameter value used in Fig. 6; and the parameter

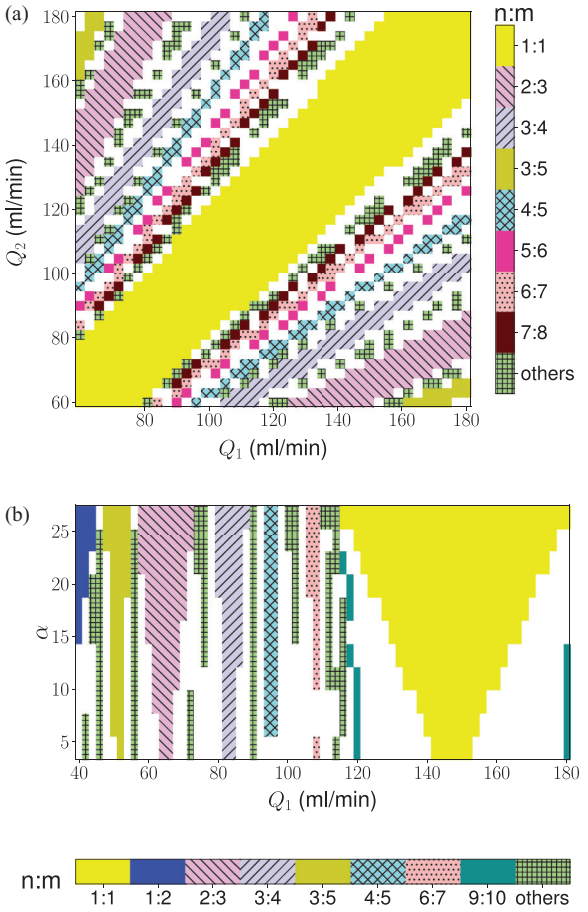

FIG. 9. (Color online) Simulated parameter spaces of the synchronized regions: (a) (Q_1, Q_2) with $\alpha = 20$ kg/m^2 s and (b) (Q_1,α) with $Q_2 = 147$ ml/min. The parameters used in these two spaces are analogous to the experimental ones shown in Figs. 6 and 7. The criteria for determining the synchronization in the simulated data were the same as used to analyze the experimental data.

space (Q_1,α) for a constant $Q_2 = 147$ ml/min is shown in Fig. 9(b).

The parameter space (Q_1, Q_2), shows the same pattern as the experimental one: we have the 1:1 synchronization around the diagonal $Q_1 = Q_2$, and the higher-order synchronizations appearing symmetrically above and below the diagonal. The simulated parameter space (Q_1,α) presents the same Arnold tongue profile with the widths of the tongues growing as the coupling strength increases, in a similar way as in the experimental parameter space (Q_1, H). The simulated parameter space presents a small difference from the experimental ones: the width growth of the 1:1 synchronization with solution height H in the experimental parameter space is not linear like the coupling strength α in the simulated parameter space, but there is no reason to expect that the function $\alpha(H)$ would be linear. For example, if the coupling were proportional to the boundary layer of the bubbling stream, we would have $\alpha \propto \sqrt{H}$, as the size of the boundary layer is proportional to the square root of the length of the bubble stream [21].

IV. CONCLUSIONS

We observed that two bubble trains, generated in nozzles with independent airflow control systems, present complex behavior. We constructed bifurcation diagrams of the times between successive bubbles $T_i^{(k)}$ vs Q_1 by varying the airflow of nozzle 1 while keeping the other constant. These diagrams presented many regions in which the dynamics of both bubblings became simultaneously periodic. We constructed two kinds of parameter space (Q_1, Q_2): (a) the periodicity parameter space, using the times between bubbles to identify the periodicities, and (b) the phase synchronization parameter space, using the microphone signals to estimate the phase difference of each pressure wave inside the hose connections. Comparing these two parameter spaces, we found that the system synchronizes in $n:m$ phase synchronization, with bubbling periodicities $P_2 = n$ and $P_1 = m$ that depend on the airflows Q_1 and Q_2. In the parameter space (Q_1, H), we observed that the width ΔQ_1 of each synchronization mode is a crescent-shaped function of the height H as in Arnold tongues. The simulations were performed with a single-nozzle model for each bubbling stream and insertion of a simple symmetrical coupling between the two bubblings, proportional to the bubble growth velocities, was enough to describe the main features of the experimental observations.

ACKNOWLEDGMENTS

We thank the São Paulo State Agency FAPESP and the Federal Brazilian Agency CNPq for financial support.

[1] A. Pikovsky, M. Rosenblum, and J. Kurths, *Synchronization: A Universal Concept in Nonlinear Sciences* (Cambridge University Press, Cambridge, 2001).
[2] L. Glass, Nature (London) **410**, 277 (2001).
[3] B. Blasius, A. Huppert, and L. Stone, Nature (London) **399**, 354 (1999).
[4] M. Rosenblum, G. Kuuz, and B. Pompe, in *Nonlinear Analysis of Physiological Data*, edited by H. Kantz, J. Kurths, and G. Mayer-Kress (Springer, Berlin, 1998), pp. 283–306.
[5] C. Schäfer, M. G. Rosenblum, H. H. Abel, and J. Kurths, Phys. Rev. E **60**, 857 (1999).
[6] D. Terman, N. Kopell, and A. Bose, Physica D **117**, 241 (1998).
[7] A. Bose, N. Kopell, and D. Terman, Physica D **140**, 69 (2000).
[8] C. C. Chow, Physica D **118**, 343 (1998).
[9] K. M. Cuomo and A. V. Oppenheim, Phys. Rev. Lett. **71**, 65 (1993).
[10] A. Argyris, D. Syvridis, L. Larger, V. Annovazzi-Lodi, P. Colet, I. Fischer, J. Garcia-Ojalvo, C. R. Mirasso, L. Pesquera, and A. Shore, Nature (London) **438**, 343 (2005).
[11] A. Tufaile and J. C. Sartorelli, Phys. Lett. A **275**, 209 (2000).
[12] A. Tufaile and J. C. Sartorelli, Phys. Lett. A **287**, 74 (2001).

[13] V. S. M. Piassi, E. Colli, A. Tufaile, and J. C. Sartorelli, Chaos Solitons Fractals **41**, 1041 (2009).
[14] A. A. Kulkarni and J. B. Joshi, Ind. Eng. Chem. Res. **44**, 5873 (2005).
[15] S. Xie and R. B. H. Tan, Chem. Eng. Sci. **58**, 4639 (2003).
[16] M. Ruzicka, J. Drahos, J. Zahradník, and N. H. Thomas, Chem. Eng. Sci. **55**, 421 (2000).
[17] P. Snabre and F. Magnifotcham, Eur. Phys. J. B **4**, 369 (1998).
[18] F. A. C. Pereira, E. Colli, and J. C. Sartorelli, Chaos **22**, 013135 (2012).
[19] J. C. Sartorelli, W. M. Gonçalves, and R. D. Pinto, Phys. Rev. E **49**, 3963 (1994).
[20] See Supplemental Material at http://link.aps.org/supplemental/10.1103/PhysRevE.87.022917 for a movie of bubbling at 2:3 synchronization. The movie was taped at 500 frames/s and shown at 25 frames/s.
[21] P. Snabre and F. Magnifotcham, Eur. Phys. J. B **4**, 379 (1998).